**ORIGINAL ARTICLE**

# Utilising of water hammer effect for surface roughening of Ti6Al4V

Dagmar Klichova[1] · Akash Nag[2] · Jakub Poloprudský[3] · Josef Foldyna[1] · Frank Pude[4,5] · Libor Sitek[1] ·
Sergej Hloch[1,6]

## Abstract

There are many technological ways to activate biocompatible surfaces, but in some cases, there are not reliable for elderly patients. It has been found that surfaces created using pulsating water jets have a structure similar to trabecular bone structures. Such a similar shape to the endoprosthesis stems would enable faster fixation. The paper presents a novel way of utilizing the water hammer effect caused by forced multiple droplet impingement with a spatial frequency of 40,000 i/s on Ti6Al4V titanium alloy surface under different technological conditions. The objective was to create a structured surface with desired values of surface profile parameters Ra and Rz to increase the possible potential for implant osseointegration, fixation and stability. Pulsating water jet was generated at pressures from 20 to 100 MPa using a circular nozzle with a diameter of 1.32 mm. Two different strategies of the jet trajectory, namely linear and cross-hatch strategy, were investigated. Results were compared with grit blasted followed by plasma spray-coated femoral stem for cementless total hip arthroplasty. It has been found that variation in the input parameters results in significant changes in the surface generated. Samples whose surfaces were generated using energy intensity lower than 5 KJ/mm$^2$ and have surface roughness in the range Ra = 4 – 8 µm were selected for surface topography and morphology analysis along with the commercial femoral stem. SEM analysis revealed the absence of foreign contamination and steeper surface heights on pulsating water jet treated samples compared to standard femoral prosthetic. The cross-section images showed the presence of sub-surface voids and craters of different sizes due to the jet's action. Surface topology is similar to trabecular shape. This indicates that roughening the surface increases the surface area and thus has potential bone tissue ingrowth during osseointegration.

**Keywords** Surface activation · Implants · Pulsating water jet · Titanium alloy · Surface roughness · Trabecular shape

## 1 Introduction

Due to the increase in the demand for hip joint replacements in the recent decade, the quality of the orthopedic prosthesis and implants are the subject of constant research so that, in the ideal case, it is not necessary to perform a reoperation. The main quality feature of an endoprosthesis is its surface which remains in direct contact with the bone tissue. Osseointegration depends on the implant surface's physical and chemical interaction with the bone tissue [1, 2]. Biological responses can be triggered by surface modifications which can guide the cellular response at the bone-implant interface supporting osseointegration [3]. Therefore, the surface properties majorly affect the complex cell behavior at the interface in vivo and in vitro applications [4]. It has been observed that osseointegration is also influenced by the surface area available with the implant. Studies suggest that a larger contact area between the implant and tissue

✉ Sergej Hloch
  sergej.hloch@tuke.sk

[1] The Czech Academy of Sciences, Institute of Geonics,
   Poruba, Ostrava, Czech Republic

[2] Faculty of Mechanical Engineering, VSB-Technical
   University of Ostrava, Poruba, Ostrava, Czech Republic

[3] Institute of Physics of Materials, Czech Academy
   of Sciences, Brno, Czech Republic

[4] Institute of Machine Tools and Manufacturing (IWF), ETH
   Zürich, Zürich, Switzerland

[5] Steinbeis High-Pressure Waterjet Technology Consulting
   Centre, 86497 Horgau, Germany

[6] Faculty of Manufacturing Technologies, Technical University
   of Kosice with a seat in Presov, Presov, Slovakia

is advantageous for the enhanced mechanical anchorage of cell adhesion compared to a smooth surface [5–7]. This increased surface area can be linked to the surface roughness of the implant surface, which further affects the osseointegration rate and biomedical fixation [8]. The surface roughness generated on the titanium surface has been classified into three levels, namely macro (10 μm – 1mm) [9], micro (1 – 10 μm) [10] and nano-sized (10 – 20 nm) scale features [11]. Each roughness level has its own significance, which promotes stronger bonding between the bone tissue and the implant surface.

Various surface modification techniques have been developed to modify titanium, and its alloys surface to be efficiently used for biomedical applications [12]. All these methods can be divided mainly into three approaches: mechanical, chemical and physical methods. Mechanical methods such as machining [13] and surface blasting [14] are commonly used for roughening surfaces. Chemical methods involve acid etching and anodization [15], improving the surface's biocompatibility. Physical methods such as plasma spray and ion implantation [16] also enhance wear, corrosion resistance, and biological activities. In the mechanical method, the most commonly used method is grit blasting with ceramic particles ($Al_2O_3$, $ZrO_2$ and $SiO_2$) to generate rougher surfaces [17]. Also, due to the action of particle impact, severe plastic deformation is induced, and an increase in the subsurface hardness and compressive residual stresses near the impacted surface is observed [18]. However, during this process many surface defects are created along with the embedment of the grit particles into the material surface, which later acts as fatigue crack nucleation points [19]. Therefore, the net effect usually decreases the implant's fatigue life which is the primary concern for load-bearing components [20]. An alternate surface roughness generation method in the form of waterjet treatment was introduced to overcome the problems caused by the inclusion of particles into the implant surface [21]. This method is further advantageous in being a cleaner and more sustainable method than grit blasting, with no need for extra precaution for dust formation, grit handling and disposal [22, 23]. Biomaterials treated with waterjet generated desired surface roughness with hardened subsurface without compromising the material's fatigue strength [24]. Utilization of abrasive particles entrained in water jet showed better surface roughness generation and induction of residual stress increasing the fatigue life of the component [25]. Several studies have been conducted on using continuous water jet (CWJ) and abrasive water jet (AWJ) to generate surface roughness and improve the fatigue strength of the implant materials such as TI6Al4V and AISI316L [26–28]. However, the major shortcoming of these studies is the utilization of high–pressure input water supply (200 – 400 MPa) in the case of CWJ, which requires regular maintenance of pumps and delivery systems. Moreover, the usage of abrasive particles remains embedded into the material's surface even after using ultrasonic cleaner and contaminate the surface [29, 30]. Also, the disposal and recycling of the used abrasive grains is a more significant challenge leading to increased surface treatment costs.

It was observed that the multiple droplet impingement causes impact pressure $p_i$ and lateral outflow. It affects the material integrity significantly compared to the stagnation pressure [31, 32] $p_s$. The water droplet impinges the material with impact pressure whose magnitude majorly depends upon the liquid's velocity and lasts for a few milliseconds [33, 34].

A method for utilisation of impact pressure – the ultrasonic pulsating water jet was patented at the Institute of Geonics, Czech Republic [35, 36]. Pulsating water jet (PWJ) act as a pulsating jet on the material surface. In this current setup, ultrasonic actuation of oscillating sonotrode induces high–pressure pulsation in the continuous water flow upstream of the nozzle, which then exits the nozzle transforms into velocity fluctuation leading to pulsating jet [37]. Ultrasonic generators generate the ultrasonic actuation with a nominal frequency. The repetitive loading of the material with water droplets does not allow mechanical relaxation of the material and leads to its fatigue failure at relatively low pressures [38]. Advantage make PWJ a suitable method for material disintegration and surface treatment or peening applications. Previous studies on utilizing PWJ for surface peening of AISI 304 samples revealed that both microhardness and induction of compressive stresses [39] near the treated surface increased significantly compared to the original sample [40, 41]. The micro-hardness and compressive residual stress values increase due to the subsurface grain refinement and increase in the grain dislocation densities acting as a barrier for further fatigue crack propagation near the peened area. Another study showed the influence of different treatment trajectory patterns, such as linear and cross-hatch pattern trajectories, during surface treatment of aluminium alloy [42]. The study focused on surface roughness and increased microhardness influenced by the pattern trajectory, traverse speed and supply pressure.

It has been found that the surface morphology and its structure are roughened [43] due to the action of impact pressure and lateral flow, which penetrates deeper into the material by creating microcavities [44]. The morphology [45–47] resembling the trabecular surface of the bone. It induced the possibility of creating a compact endoprosthesis, the surface of which would be modified by a pulsating water jet. It allows a simpler production of femoral stems compared to plasma spraying layer. A preliminary study was carried out by the same group, where Ti6Al4V samples were exposed to the action of PWJ with supply pressure, $p = 70$ MPa using nozzle diameter, $d = 0.8$ mm [48]. In order to

enable faster traverse speed compared to [48] pressure $p =$ 100 MPa pressure has been used.

## 2 Experimental set up

Titanium and its alloy are now commercially used as implant materials for their use in dental and orthopaedic implant applications. This increased acceptance of titanium alloys is attributed to enhanced properties such as excellent corrosion resistance, mechanical strength, elastic modulus and biocompatibility properties which are closest to bone properties as compared to other commercially available materials

[49–51]. Therefore, Ti6Al4V titanium alloy (Grade 5) material was selected to study surface roughening through the pulsating water jet. Testing samples with the dimension of 20 x 20 mm were cut from a 5 mm thick sheet by an abrasive water jet. Subsequently, silicon carbide abrasive sandpapers were used to polish the top surfaces underwater (the last sandpaper with a grit size of 1200 corresponds to the average abrasive grain size of 15 μm). Basic chemical composition and elemental mapping of the titanium alloy are obtained through EDS analysis and in shown in Fig. 1. Mechanical properties of as received material is listed in Table 1. The surface profile roughness parameters of untreated polished sample surfaces are presented in Table 2.
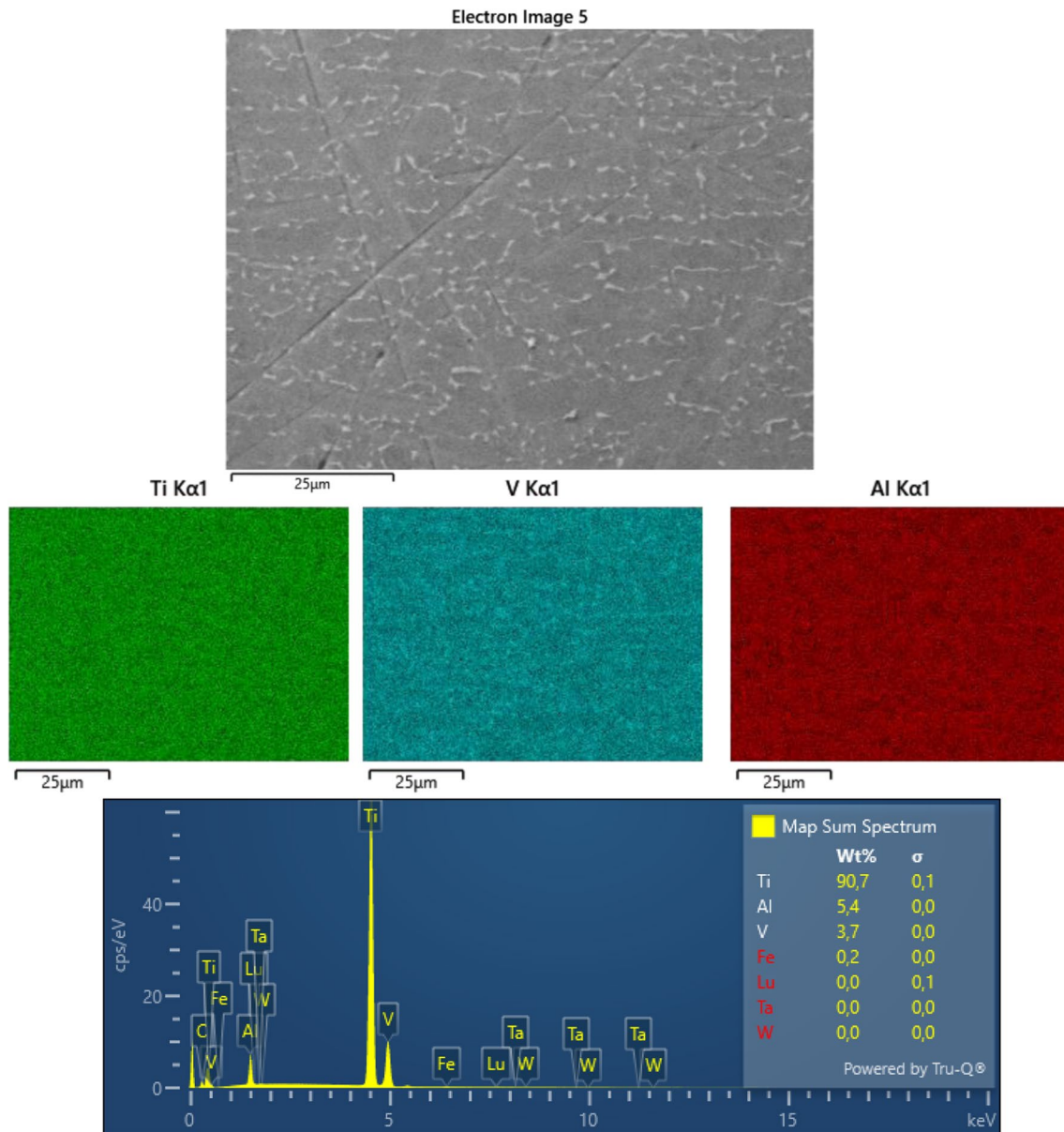


**Fig. 1** EDS elemental mapping of the Ti6Al4V alloy depicting the elemental distribution and composition of the sample

**Table 1** Basic properties of Ti6Al4V titanium alloy (Grade 5)

| Mechanical properties | | | | | |
|---|---|---|---|---|---|
| Tensile strength [MPa] | Yield strength [MPa] | Elongation [%] | Elasticity modulus [GPa] | Hardness, Brinell | Density [kg/m$^3$] |
| 895 | 828 | 10 | 114 | 334 | 4420 |

**Table 3** Operating parameters used in experiments.

| Pressure [MPa] | 20 | 40 | 70 | 100 |
|---|---|---|---|---|
| Standoff distance [mm] | 65 | 65 | 65 | 105 |
| Number of passes | 8 | 6 | 4 | 2 |
| Traversing speed [mm/s] | 5, 10 | 40, 80, 160 | 160, 240, 320 | 240, 320, 400 |

The experimental facility consisted of a high-pressure water supply system, an ultrasonic generator, a robotic manipulator for traversing the pulsating jet over testing samples and a pulsating head nozzle assembly. A plunger pump capable of delivering up to 67 l/min at an operating pressure of up to 160 MPa was used to feed the pulsating head nozzle assembly with high-pressure water [52]. The pulsating head assembly is equipped with a commercially available round jet nozzle (Stoneage Attack Tip AP4) with an orifice diameter of 1.32 mm (0.052 inches).

The pulsating nozzle head assembly consisted of a piezoelectric transducer vibrating at the operating frequency of about 40 kHz and driven by an ultrasonic generator with a maximum output power of 400 W. The piezoelectric transducer, in the form of oscillating sonotrode interacts with the high-pressure water supplied by the pump inside an acoustic chamber which is a part of pulsating nozzle head assembly. High-frequency oscillations induce pressure fluctuations in the water flow, whose amplitude enhances while propagating towards the nozzle exit. The efficient transformation of the ultrasonic input energy into output requires tuning the operating frequency into the resonance regime and can be done by variation in the acoustic chamber length. The optimal setting of the acoustic chamber length majorly depends on the flow rate of the supply water. The procedure for obtaining the optimal setting is discussed elsewhere in detail [53, 54] and was used in the current experiments to set optimal values of chamber length for all the different pressure values. After setting the acoustic chamber length, the optimal standoff distance was found out through pilot experiments. The erosion trace was created by gradually increasing the distance between the nozzle and the material surface with the help of the robotic arm. The standoff distance corresponding to the deepest eroded groove was selected as the optimal standoff distance. This pilot test was repeated for each pressure level. The operating pressures selected for the current study were $p = 20, 40, 70,$ and 100 MPa. During the experiments, traverse speed and the number of passes were varied to

achieve a wider range of surface roughness parameters (i.e., Ra from 5 to 30 µm and Rz from 40 to 180 µm) which gives the option to select optimal parameters which can produce similar surface to implant surface. Combinations of operating parameters used in the presented study are listed in Table 3.

After clamping the sample and setting the operating parameters, the nozzle was moved over the sample using a robotic manipulator according to a predefined strategy (Fig.2a). Two strategies of the nozzle movement over the sample surface were used in the experiments: linear with spacing, a = 0.2 mm (Fig. 2b) and cross-movement with the same spacing (Fig. 2b).

In total, 24 samples were treated: 22 by the pulsating water jet at various operating parameters and two by the continuous water jet, one at the operating pressure of 20 MPa at the traversing speed of 5 mm/s and another at the operating pressure of 100 MPa at the traversing speed of 240 mm/s both using the linear movement strategy.

An optical profilometer was used to measure the characteristics of the treated surface area of all samples. The surface was scanned in 10 lines. The total length of the measured line was 18 mm; the evaluated length was 12.5 mm for Ra<10 µm and 16 mm for Ra>10 µm. The spacing between the measured points was 1.5 µm. Scanning of lines was performed in two directions: direction x was parallel to the linear movement, and direction y was perpendicular to the linear movement. The measured data were analyzed according to ISO 21920-2, ISO 21920-3 and ISO 16610-21 standards.

Evaluation of surface characteristics required to consider the specific structure of the newly generated surface, which was divided into components according to the spacing of relevant roughness's. However, they changed considerably in relation to the operating parameters' setting during the experiment. Therefore, it was necessary to use different settings of the λc profile filter, which defined the boundary between roughness and waviness components [55]. The

**Table 2** Surface topography of the polished sample before experimental runs along with commercially obtained prosthetic femoral stem

| Direction | Ra [µm] | Rz [µm] | Rsk | Rku | Rsm [µm] |
|---|---|---|---|---|---|
| Polished sample (x direction) | 0.584 | 5.05 | 0.119 | 3.304 | 197.403 |
| Polished sample (y direction) | 0.567 | 4.559 | 0.131 | 3.547 | 172.908 |
| Femoral stem | 4.84 | 36.54 | -0.445 | 3.71 | 147.1 |

**Fig. 2** **a**) Experimental setup depicting various parts of the PWJ equipment, **b**) nozzle movement strategies used during the study and **c**) treated and untreated surface of Ti6Al4V sample
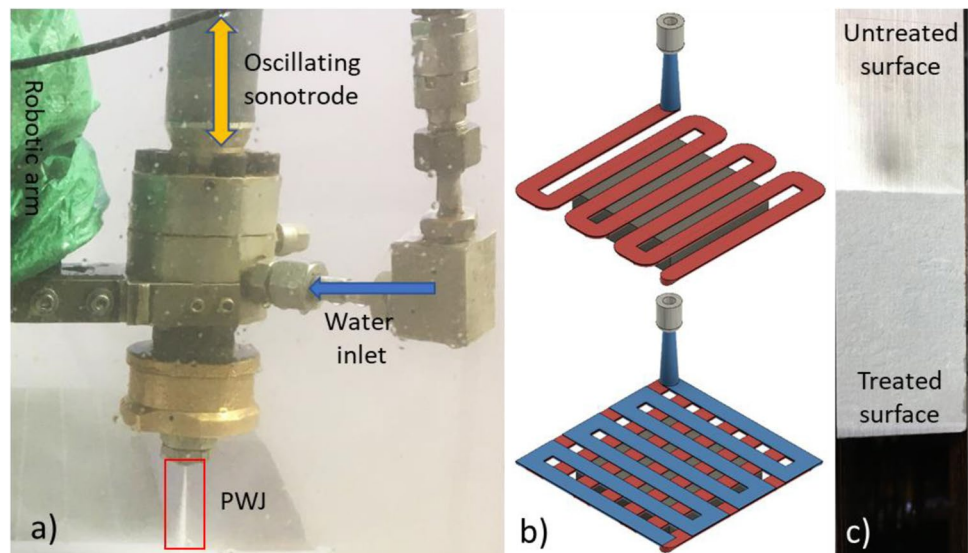
R-parameters provided the quantification of the surface under investigation. The most frequently used roughness parameters, i.e., the average arithmetic height Ra and ten-point height Rz, were used to characterize surfaces treated by the pulsating water jet.

Other monitored height parameters were the skewness Rsk and the kurtosis Rku. The skewness of the surface profile represents the degree of symmetry of the profile about the mean line, and it is sensitive to occasional deep valleys or high peaks of the profile. Profiles with deep valleys or removed peaks have Rsk <0, whereas profiles with high peaks or filled valleys have Rsk >0. The kurtosis of the profile indicates the sharpness of the probability density of the profile. Profiles with relatively many high peaks and low valleys have Rku >3, and profiles with relatively few high peaks and low valleys have Rku <3 [56].

The surfaces obtained after the PWJ treatment were compared with the commercially available femoral prosthetic surface (SL-PLUS INTEGRATION-PLUS, Make: Smith&Nephew) to understand the practical utilization of the proposed treatment method. The commercial femoral stem is forged, and corundum blasted, followed by a vacuum plasma sprayed hydroxyapatite layer of 50 μm. According to the manufacturer's datasheet, the optimal range of implant surface roughness varies from Ra = 4-8 μm. Therefore, the treated samples which satisfied the roughness range were selected further for topological and morphological investigations.

A digital microscope visualized the structure of treated surfaces. An area of 5009 μm x 5284 μm with a distance of 0.7 μm between the scanned points was examined at 300x magnification using the stitching method. The surface structure visualization of the tested samples significantly contributes to the overall surface quality evaluation by providing an accurate picture of the newly created surfaces.

For the surface morphology study, the created surfaces were also examined using scanning electron microscopy (Tescan LYRA 3 XMU FEG/SEM x FIB) to understand further the typical characteristics of the roughened surface generated by PWJ and femoral prosthetic sample [57]. The top and cross-sectional views of the generated roughened sample were observed.

## 3 Results and discussion

The effect of the movement strategy on surface roughness parameters was analyzed with respect to the surface treatment rate. The surface treatment rate $S_t$ indicates the area of the treated surface per unit time; it was calculated using the formula (1):

$$S_t = \frac{av}{n} \left[ \text{mm}^2/\text{s} \right] \tag{1}$$

where $a$ is the spacing of the nozzle movement over the sample in mm, $v$ is the traverse speed of the nozzle in mm/s, and n is the number of passes of the movement strategy.

The analysis of results indicates that tested movement strategies (linear and cross-hatched) have negligible influence on resulting surface characteristics and homogeneity of the treated surface. It also shows that the orientation of scanning lines (directions x and y) has a minor influence on evaluated surface topography parameters. Therefore, further results and analyses are presented and discussed only for the linear movement strategy and the direction x of scanning lines. An example of the effects of the different movement

strategies on Ra and Rz surface roughness parameters is presented in Fig. 3.

In addition, the surface treatment rate allows comparing the pulsating jet performance under various operating conditions used in the current study. Graphs in Figs. 4 and 5 illustrate the dependency of Ra, Rz and Rsk, Rku surface roughness parameters, respectively on the operating pressure and surface treatment rate.

The results indicate that the topography of surfaces generated by the pulsating water jet can be controlled by adequately adjusting operating parameters. The required values of surface roughness parameters can be obtained by changing the operating pressure and the surface treatment rate. The increase in the supply pressure increases the magnitude of the impact pressure induced into the material surface, leading to a higher degree of erosion. The results showed a 19-fold increase in the $Ra$ values for a four-fold increase in supply pressure, i.e., for $p = 100$ MPa with a minimum $S_t = 24$ mm$^2$/s compared to $p = 20$ MPa with $S_t = 0.125$ mm$^2$/s. This significant increase in the surface roughness values shows the influence and dominance of supply pressure over
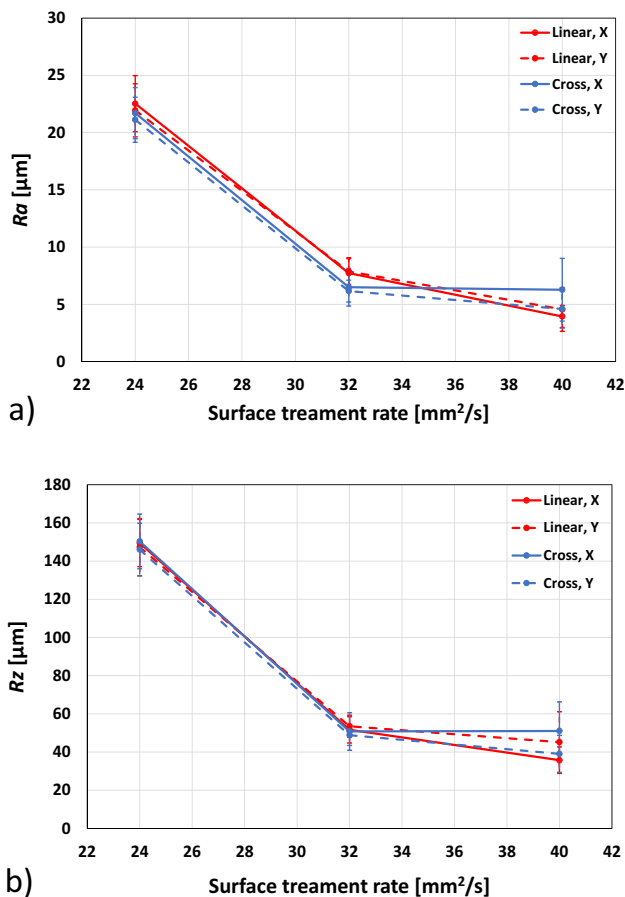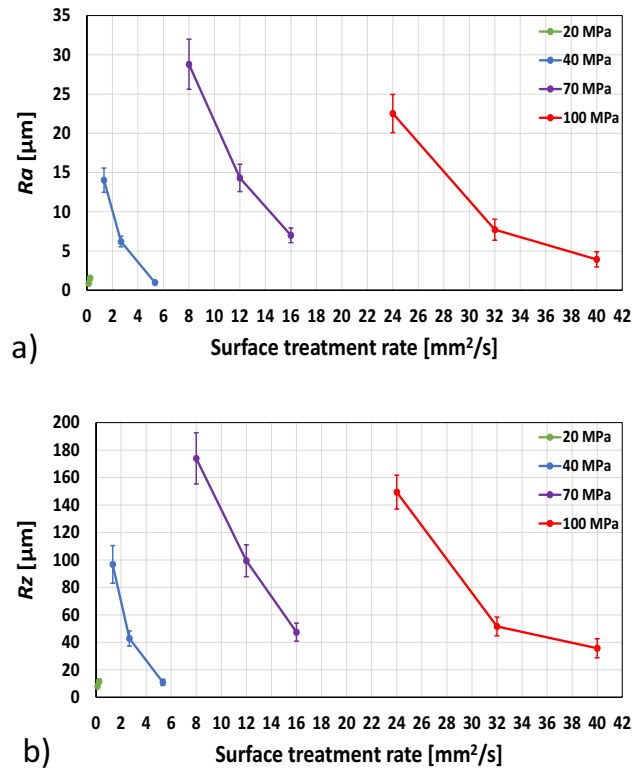


a)



b)

**Fig. 4** Effect of operating pressure and surface treatment rate on surface roughness profile parameters **a**) Ra and **b**) Rz

the erosion mechanism. Also, surface treatment rate plays a vital role as it is directly linked with time; that the treatment process would require to achieve the desired level of roughness for the entire surface at fixed supply pressure. For instance, for supply pressure, $p = 100$ MPa, $Ra$ values decrease approximately 4 – 5 folds with a nearly quarter-fold increase in surface treatment rate. The decrease in the roughness values with increased surface treatment time are due to lesser repetitive impacts per unit area of the material and lesser interaction time between the surface and the PWJ [47]. Therefore, a proper selection of parameters must be done to achieve the desired result with less treatment time. The maximum surface roughness, Rz values follow a similar trend as Ra, i.e., increases with a decrease in the surface treatment rate at constant supply pressure and with the increase in the supply pressure. However, complete information about the performance of the generated surface under biological conditions cannot be only fulfilled by just analyzing Ra and Rz surface parameters.

The cell adhesion and proliferation/differentiation leading to enhanced bone formation require a larger surface area contact between the implant material and the surrounding bone. For efficient holding of cells and bone tissues, valley formation on the material surface is required for faster osseointegration [58]. This information can be obtained using
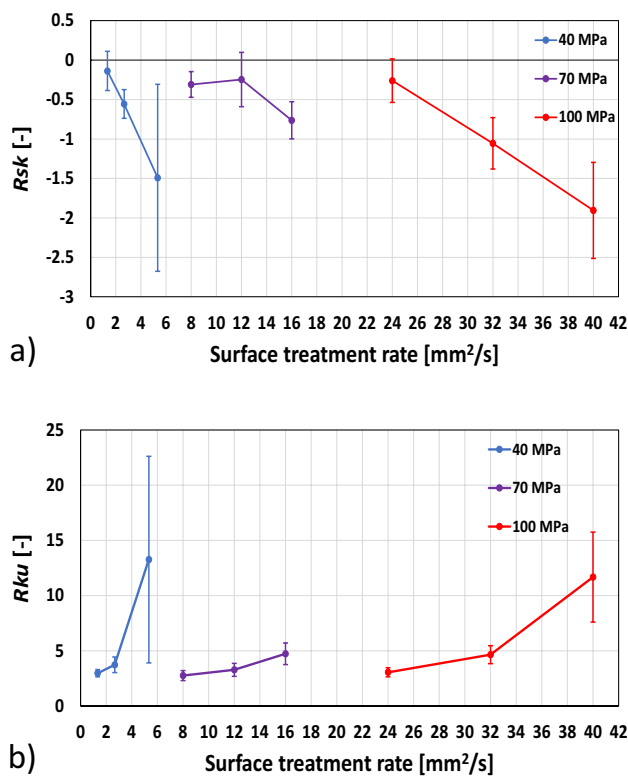


a)



b)

**Fig. 3** Influence of the trajectory strategy and orientation of scanning lines on surface roughness profile parameters **a**) Ra and **b**) Rz. Operating pressure of 100 MPa

**Fig. 5** Effect of operating pressure and surface treatment rate on surface roughness parameters **a**) Rsk and **b**) Rku

surface roughness hybrid parameters Rsk and Rku which represent the shape and sharpness of the height distribution, respectively. The results also show that values of the skewness Rsk are negative and decrease with the increasing surface treatment rate within the operating parameters of the experiment. This trend indicates that deep valleys and rounded peaks are characteristic of surfaces created by PWJ under the given operating conditions. The absolute value of the Rsk increases with an increase in the input supply pressure due to higher hydraulic power possessed by the PWJ, which when impacts the surface, causes the removal of the asperities initially present on the surface. The skewness Rsk values of all the generated surfaces are lower than the original or untreated sample surface (Rsk = 0.119 μm). This observation of achieving lower Rsk values can be attributed to the action of the lateral jetting occurring after the impact of the water clusters. In this phase, the water droplet spreads parallel to the material surface with velocity estimated to be 10 times the impact velocity and possess sufficient energy to tear off all the surface asperities present in the form of peaks to generate rounded or truncated peaks. As Rsk values are sensible to the deviation of the symmetry of peaks and valleys above and below the mean line, therefore for rounded peaks and deep valleys higher negative values are observed for PWJ treated surface as compared to original surface.

Also, it can be observed that more negatively skewed surface values are achieved by increasing surface treatment rate at fixed supply pressure, pointing to the creation of rounded or worn-out peaks. Lower values of Rsk are also attributed to the increased load-bearing conditions of the surfaces due to flattened peaks which provide better contact conditions for the Ti implant and the surrounding bone tissues, promoting osseointegration [59].

On the other hand, the kurtosis Rku measured for the generated surfaces are close to or higher than three, indicating that the surfaces created by pulsating water jet have relatively many sharp peaks and valleys. These values represent that most of the material lies near the mean plane of the material, along with sharper peaks and valleys spread throughout the treated surface. Therefore, it can be concluded that the surfaces generated by the action of PWJ under different experimental conditions are advantageous for the efficient osseointegration, fixation and osteoblast differentiation in vitro and bone-implant contact in vivo leading to faster healing of wounds. It should be noted that the continuous water jet generated under the same operating conditions has virtually no effect on the surface roughness of titanium alloy samples. Utilization of the pulsating water jet for surface roughening increases the surface treatment rate up to ten times compared to the results obtained using the continuous water jet at the pressure of 360 MPa reported by Barriuso et al. [22].

The energy intensity of any process is a critical parameter that indicates the amount of energy per unit area of the material required to achieve desired results. The energy intensity of the process of PWJ surface roughening was assessed through energy consumption per unit area treated $E_C$. The energy consumption was calculated using the equation (2):

$$E_C = \frac{W_h}{S_t} \left[ \text{kJ/mm}^2 \right] \tag{2}$$

where $W_h$ is the hydraulic power of the jet in kW and $S_t$ is the surface treatment rate in mm$^2$/s.

The energy intensity of the PWJ used for surface roughening is illustrated in Fig. 6. It shows that the application of the PWJ generated at higher pressure decreases the energy consumption of the roughening process if similar surface roughness parameters values are to be obtained. Although the hydraulic power of the PWJ for $p = 100$ MPa ($W_h = 55$ W) is 11 times more than $p = 20$ MPa ($W_h = 5$ W), the surface treatment rate used for achieving the desired range of surface roughness with $p = 100$ MPa ($S_t = 40$ mm$^2$/s) is 160 times more than $p = 20$ MPa ($S_t = 0.25$ mm$^2$/s). A significantly higher value of surface treatment rates makes surface treatment using $p = 100$ MPa most energy efficient, followed by 70 and 40 MPa. Rz also shows a similar trend as Ra for all experimental runs (Fig. 6b).
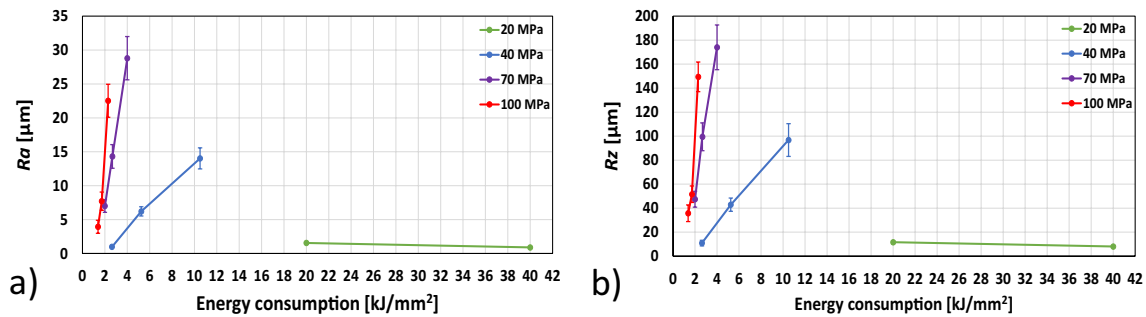
**Fig. 6** Energy intensity of the process of pulsating water jet surface roughening with respect to the operating pressure and surface roughness parameters, **a**) Ra and **b**) Rz

The surface roughness values obtained by the action of PWJ were compared with commercially available femoral Titanium alloy prosthetic. The Ra and Rz of the sample were measured to be $4.84 \pm 0.08$ µm and $36.54 \pm 0.32$ µm, respectively, which lies within the optimal range specified by the manufacturer, i.e., Ra = 4 – 8 µm. Similar roughness values were obtained on surfaces generated by PWJ with $p = 100$ MPa with $S_t = 40$ and 32 mm$^2$/s, $p = 70$ MPa with $S_t = 16$ mm$^2$/s and $p = 40$ MPa with $S_t = 2.67$ mm$^2$/s. Also, the energy intensities of the PWJ required to achieve these surface roughness's are below 6 kJ/mm$^2$, making the proposed method energy efficient. Further, the mean Rsk value of the femoral prosthetic sample was measured to be -0.445 as compared to -0.246 to -1.905, corresponding to the selected treated samples, attributing to the presence of flattened peaks and deeper valleys required for better osseointegration and enhanced load–bearing capability. Also, higher Rku = 3.272 – 11.67 was obtained for the treated sample compared to the mean Rku = 3.71 for the femoral prosthetic sample, showing the sharpness of the height profile of the surfaces obtained through the action of PWJ. Surface topography and morphology were investigated for further investigation and comparison of the surfaces generated by the PWJ of the selected samples with commercially obtained Ti femoral prosthetic sample surface.

The surface topographies created by the action of the PWJ are documented in Fig. 7. It shows surfaces produced by PWJ generated at $p = 100$ MPa with $S_t = 40$ mm$^2$/s (Fig. 7a) and 32 mm/s (Fig. 7b), $p = 70$ MPa with $S_t = 16$ mm$^2$/s (Fig. 7c) and $p = 40$ MPa with $S_t = 2.67$ mm$^2$/s (Fig. 7d). For comparison surface of femoral prosthetic sample was also analyzed (Fig. 7e). For each treated sample, an isometric 3D view followed by the 2D top view and a height profile along a line randomly selected by the mean surface area is shown in Fig. 6. It can easily be observed that although Ra and Rz values of all the samples selected are similar and within the desired range of 4-8 µm, but the topographical features varies among themselves which alters its affinity to make stronger bonds with bone tissue and promote osseointegration. The sample created with $p =$

100 MPa and a $S_t = 40$ mm$^2$/s shows a roughened surface with mostly flattened peaks and a few sharp and deep valleys over the treated surface. This also correlates to the higher negative value of Rsk = -1.905, as shown in Fig. 5a. Also, the steeper valleys visualized from the surface profile, arguments the high Rku = 11.669 observed in Fig. 5b. The maximum measured valley depth was approximate twice the maximum peak height. However, the amount of surface area increased due to the induced roughness was measured to be 8.29%. With the decrease in the $S_t = 32$ mm$^2$/s, at the same supply pressure, the time interaction, or the number of impacts of the PWJ on a unit length of the material increases to 125 impingements/mm/pass. This increased number of impingements leads to the induction of higher compressive stresses into the material surface, leading to the formation of more profound local valleys spread randomly over the entire surface. The increased surface roughness affects the treated sample's surface characteristics. The valleys' width or openings are more comprehensive than the sample generated at the same operating pressure but with a higher surface treatment rate ($S_t = 40$ mm$^2$/s). This blunt height profile correlates to a lower value of Rku = 4.646 compared to 11.669 for a $S_t = 40$ mm$^2$/s. For operating pressure $p = 70$ MPa with $S_t = 16$ mm$^2$/s, the surface formed by the PWJ is similar to the surface formed with $p = 100$ MPa and $S_t = 24$ mm$^2$/s. The same surface characteristic with lower supply pressure is attributed to the increased number of passes ($n = 4$) by double compared to $p = 100$ MPa ($n = 2$). However, the surface generated has more compact and truncated peaks than spiky and sharp peaks for earlier samples. These flattened peaks enhance the load-bearing capacity of the implant, which is vital for cementless implants. Also, the formations of the deeper valleys or pits indicate more surface area for cell adhesion and differentiation. An increase in 22.27% surface area was measured due to the induced surface roughness. A smooth, uniform surface is achieved with supply pressure, $p = 40$ MPa and $S_t = 2.67$ mm$^2$/s. This surface is generated by uniformly spread peaks and valleys formed by the action of the PWJ overall the surface. The surface generated is similar to a typical surface generated by the action of the repetitive impact
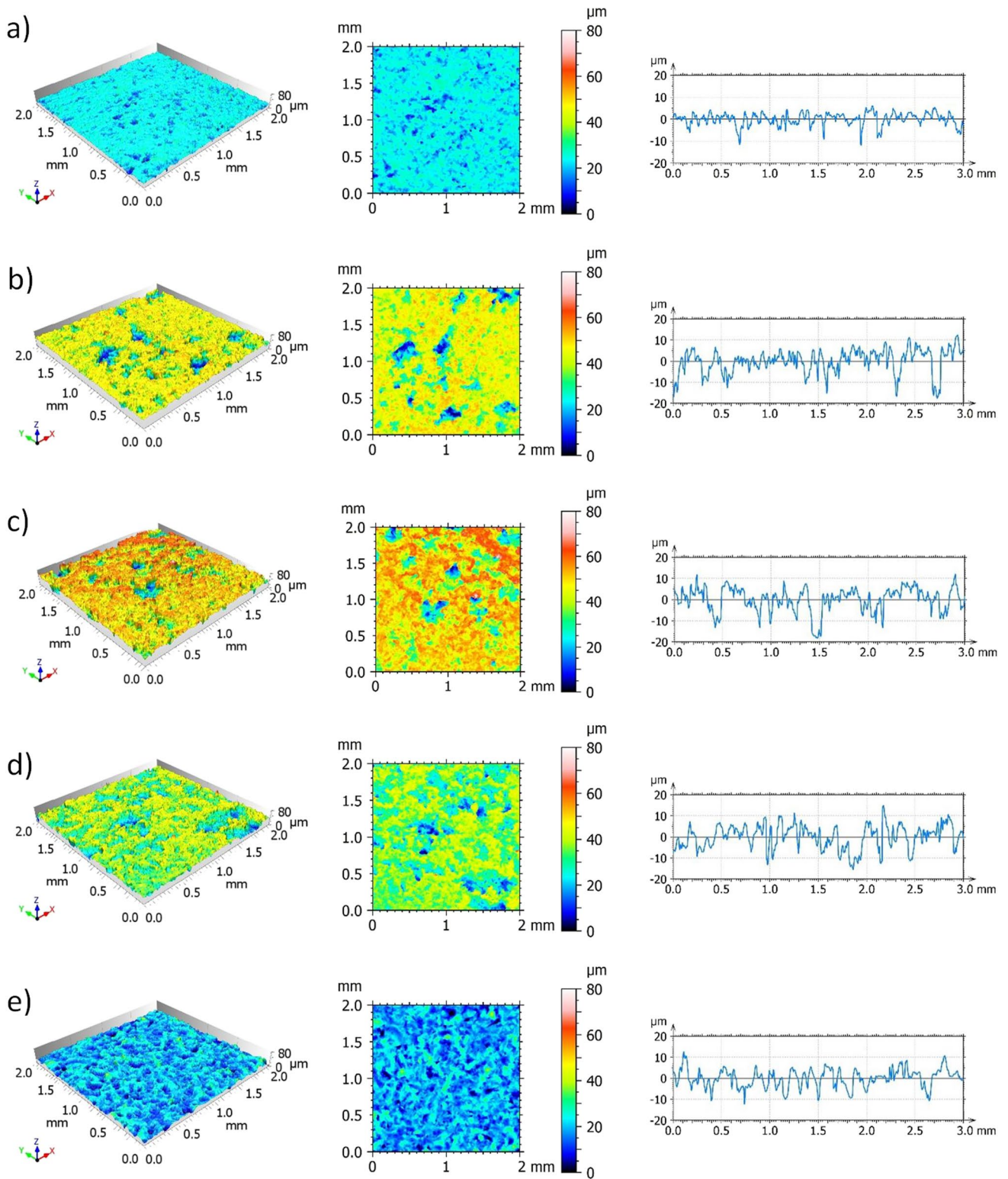
**Fig. 7** Surface topography (3D view, top view and line profile) of the selected samples generated with parameters **a)** $p = 100$ MPa, $S_t = 40$ mm$^2$/s, **b)** $p = 100$ MPa, $S_t = 32$ mm$^2$/s, **c)** $p = 70$ MPa, $S_t = 16$ mm$^2$/s, **d)** $p = 40$ MPa, $S_t = 2.67$ mm$^2$/s and **e)** Femoral prosthetic sample

of the water clusters. It is less negatively skewed and has a smoother formation of valleys and peaks. Surface topography of commercially acquired implant surface was also observed. Stable and uniform surface characteristics were observed. Similar heights of peaks and valleys were measured for the generated surface, with valleys slightly deeper than the peaks. The surface represents a typical peened surface using any conventional treatment method. The mean values of Rsk and Rku were measured as -0.445 and 3.710, respectively. These values indicate that the surface mainly consists of deeper valleys and rounded peaks. However, higher magnitudes of both the parameters were obtained on the selected sample, generated by the action of PWJ, showing the efficiency of creating a surface inclined towards potential efficient osseointegration.

Fig. 8 shows a closer inspection of the surface of the standard femoral prosthetic compared to surfaces created by four different process parameters of PWJ. A closer look at the hip prosthetic shows contamination embedded inside the base material (Fig. 8). Elemental analysis of the contamination obtained through EDS technique shown in Fig. 9 infer it to be corundum particle used during the grit blasting of the prosthetic surface. The presence of these impurities also affects the surface roughness and topology of the conventionally manufactured prosthetic implant,

which in turn affects its service lifetime. The surface also shows a high number of scratch marks. The scratch marks have different directions at each location on the surface. This creates visible boundaries between regions are created either by sharp down valleys or pilled-up material peaks. The PWJ-created surface does not show similar scratch marks anywhere. The sample created with $p = 100$ MPa and $S_t = 40$ mm$^2$/s shows a relatively even surface riddled with cracks and stochastically distributed cavities. The other samples created with different parameters show significantly wider cavities. The sample formed with $p = 100$ MPa and $S_t = 32$ mm$^2$/s shows a deep cavity connected to several surrounding cavities by a network of cracks. The sample also shows smooth surfaces on the rounded peaks and bottom of the cavities. There are also visible smooth areas, especially inside or close to cavities entrances on samples created with $p = 70$ MPa with $S_t = 16$ mm$^2$/s and $p = 40$ MPa with $S_t = 2.67$ mm$^2$/s. These can be attributed to lateral outflow jetting. The sample with $p = 70$ MPa shows a network of cracks across the whole area from the cavity on the right to the cavity on the left. The sample formed with $p = 40$ MPa shows a similar crack network. However, the number of cracks are opened so wide that they can be considered cavities. This figure also shows a smooth area on
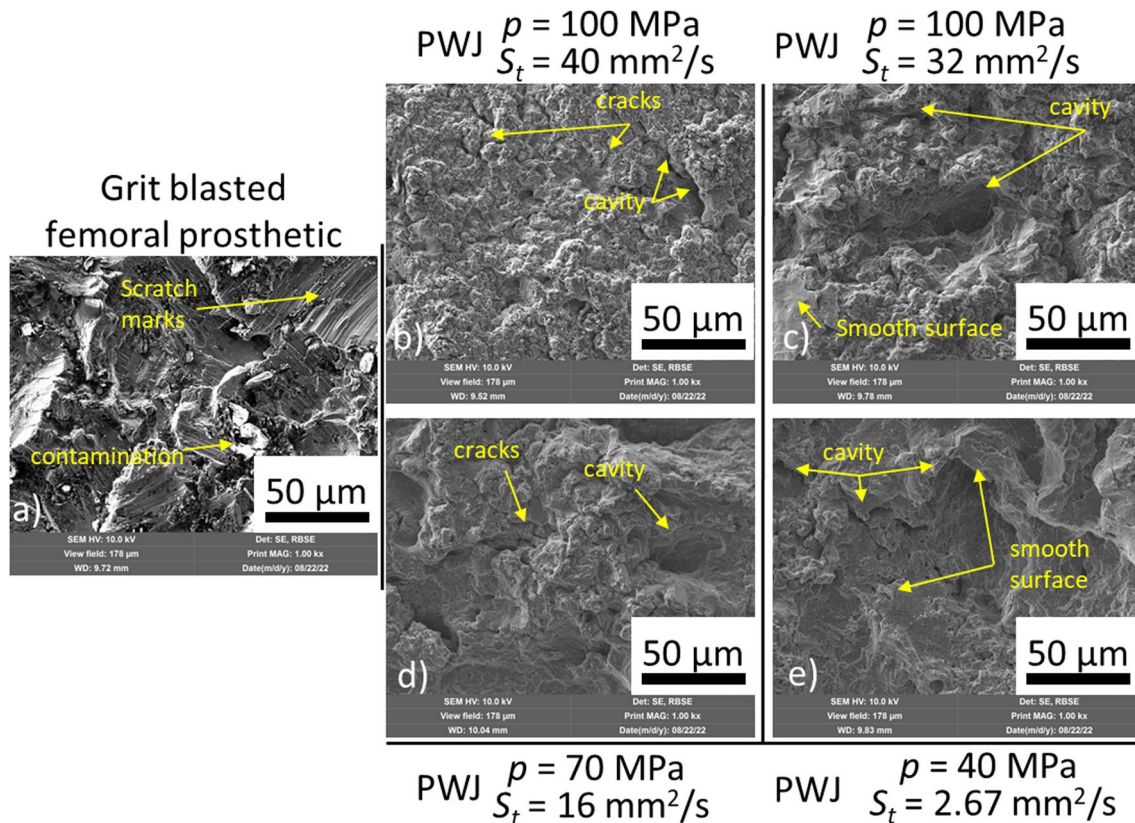


**Fig. 8** Top view of **a**) grit blasted femoral prosthetic compared to the top view of samples roughened by PWJ with **b**) $p = 100$ MPa and $S_t = 40$ mm$^2$/s, **c**) $p = 100$ MPa and $S_t = 32$ mm$^2$/s, **d**) $p = 70$ MPa and $S_t = 16$ mm$^2$/s and **e**) $p = 40$ MPa and $S_t = 2.67$ mm$^2$/s
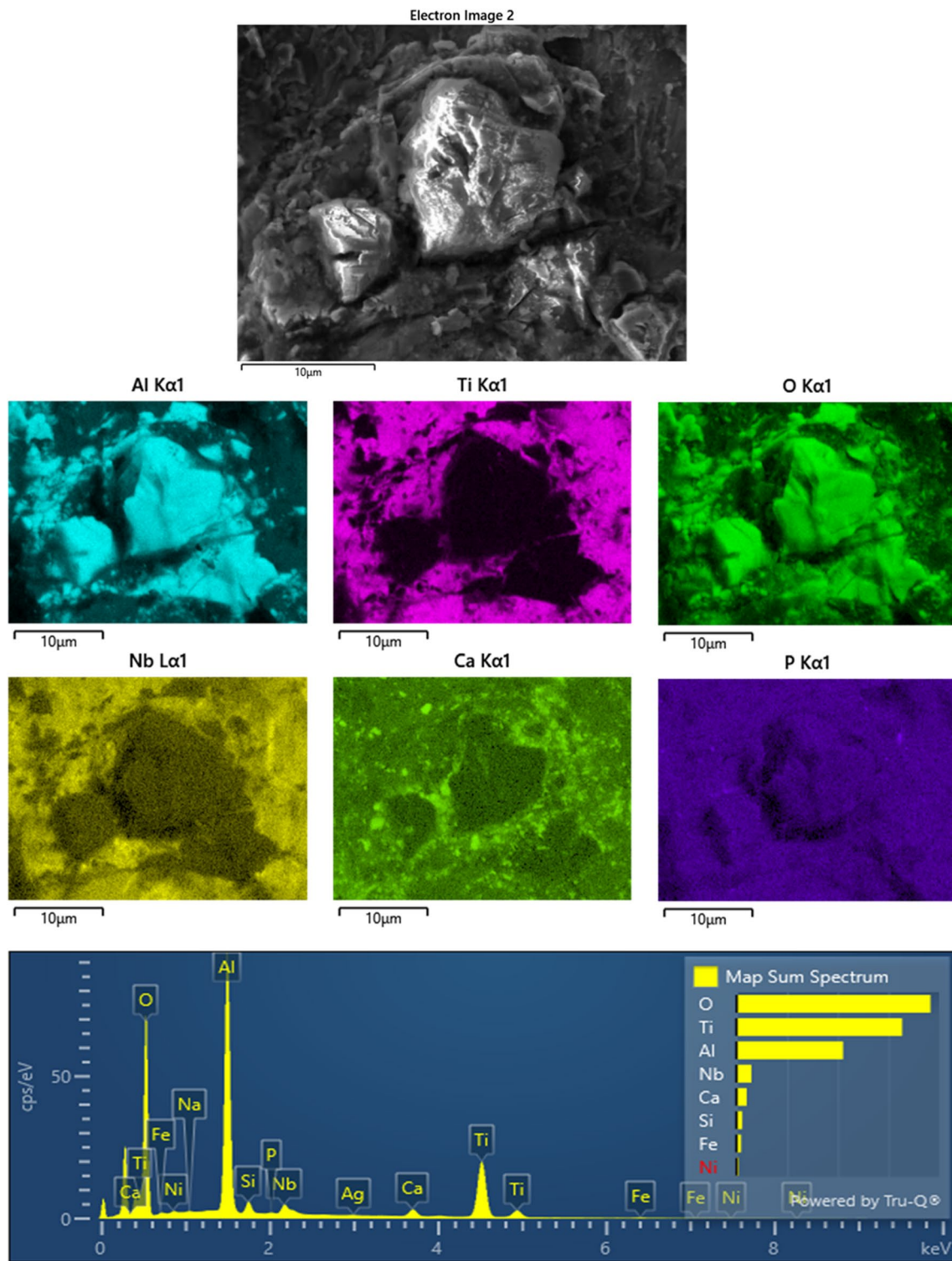
**Fig. 9** EDS elemental mapping of the surface contamination of the femoral prosthetic highlighted in Fig. 8 depicting the elemental distribution and composition of the sample

the top of the cavity entrance, which can be either caused by lateral outflow or plastic deformation of the material. These rounded peaks observed using SEM are correlating with

lower Rsk values. The rounded peaks show lesser stress concentration due to smoother surface transition compared to sharp angle edges [60, 61]. This promote the load bearing

capacity of the femoral prosthetic implants. Therefore, compared to the surface of a standard femoral prosthetic, the surface created under the action of PWJ shows gradual peaks and craters between the areas, along with no foreign particle contamination and scratch marks leading to the creation of steep height differences over the surface. The PWJ samples show a number of deep and wide cavities or valleys with trimmed or rounded smooth peaks suitable for osseointegration.

The cross-section of the standard femoral prosthetic (Fig. 10) shows detail of the pit created on the surface. The pit has a diameter of about 113 µm. Both edges of the pit are riddled with narrow cracks. The cross-section of the sample formed with $p = 100$ MPa and $S_t = 40$ mm$^2$/s shows a roughened surface with a wavy profile, and the top of the surfaces are usually concentrators for crack initiation. The cross-section also shows a large sub-surface void [44] connected to the surface only by a small crack. This void may be connected to the surface in a different place than the cross-section through micro-tunnels. Sample with $p = 100$ MPa and $S_t = 32$ mm$^2$/s show crack initiating on the material peaks and valleys. Some cracks reach a width to be considered cavities. A sample cross-section created with $p = 70$ MPa shows

wider cavities going into the side of the upheaved material. These lateral cavities can be beneficial for endoprosthesis as an anchor point for osseointegration. The cross-section of the sample formed with $p = 40$ MPa shows both subsurface voids connected to the surface by small cracks. The figure also shows lateral cracks and one lateral crack widening on the entrance. The main difference observed in the cross-section of the standard femoral prosthetic and the surfaces created by PWJ is the creation of a wider range of shapes and sizes of pits compared to the uniform size in the femoral prosthetic. Also, the cracks generated by the action of PWJ can propagate under the material through micro-tunnels to form sub-surface voids, which can be favorable sites for enhanced osseointegration.

## 4 Conclusions

The preliminary study of surface roughening of Ti6Al4V titanium alloy (Grade 5) by PWJ showed that the resulting surface topography could be controlled by adequately adjusting operating conditions. Some of the important observations of the results are concluded as follows:
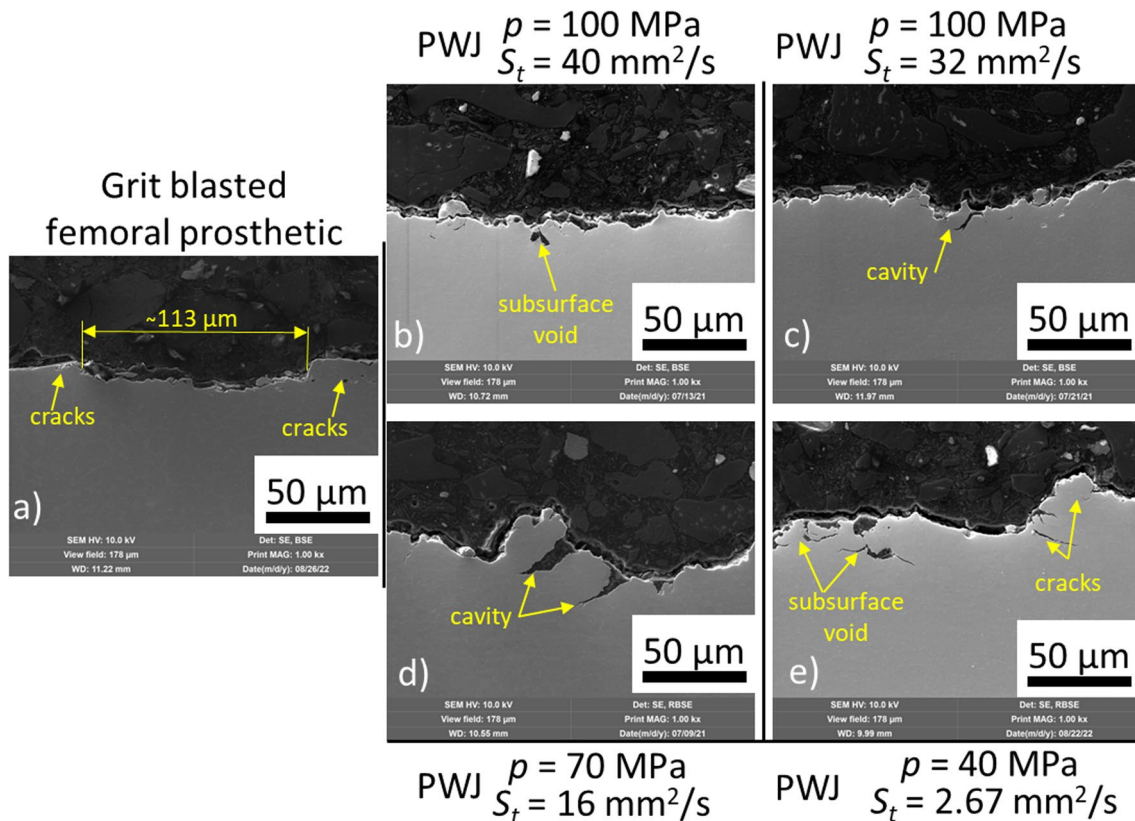


**Fig. 10** Cross-section of **a**) grit blasted femoral prosthetic compared to the top view of samples roughened by PWJ with **b**) $p = 100$ MPa and $S_t = 40$ mm$^2$/s, **c**) $p = 100$ MPa and $S_t = 32$ mm$^2$/s, **d**) $p = 70$ MPa and $S_t = 16$ mm$^2$/s and **e**) $p = 40$ MPa and $S_t = 2.67$ mm$^2$/s

1) Surface roughness parameters depend upon the surface treatment rate, i.e., increasing the $S_t$ values at constant $p$ values results in a sharp decrease in the roughness values (Ra and Rz). This is attributed to the lower inter-action time between the PWJ and the material surface.

2) Lower values of Rsk were observed for higher pressure values ($p = 100$ MPa) compared to lower pressure ($p = 40$ MPa). This is due to the rounding of the surface peaks and the formation of deeper cavities with a higher magnitude of lateral jetting and impact velocity corresponding to higher pressure values.

3) Increasing the operating pressure lowers energy consumption per unit area if the same surface roughness parameters are to be obtained.

4) Surface morphology results showed similar surface topographies of the samples generated by PWJ compared to commercially available femoral stem. The images also depicted the distribution of the peaks and valleys throughout the material surface after the PWJ treatment.

5) SEM images of the top surfaces showed the absence of surface contamination (inorganic abrasive particles) and steep height difference on the material surface due to scratch marks on the PWJ-treated samples compared to the standard femoral prosthetic sample. Cross-section images showed the formation of sub-surface voids and craters in the PWJ-treated samples, which can be potential sites for tissue anchorage promoting osseointegration and reservoir for additional hydroxyapatite or medicaments.

Further research should focus on wettability and cell growth test on the generated samples to confirm the adequate surface characteristics and parameter levels in terms of osseointegration, fixation, and stability of endoprostheses.

## Declarations

**Ethics approval** The research does not involve human participants or animals and the authors warrant that the paper fulfils the ethical standards of the journal.

**Consent to participate** It is confirmed that all the authors are aware and satisfied of the authorship order and correspondence of the paper.

**Consent for publication** All the authors are satisfied that the last revised version of the paper is published without any change.

**Competing interests** The authors declare no competing interests.

## References

1. Kieswetter K, Schwartz Z, Dean DD, Boyan BD (1996) The role of implant surface characteristics in the healing of bone. Crit Rev Oral Biol Med 7:329–345

2. Annunziata M, Guida L (2015) The effect of titanium surface modifications on dental implant osseointegration. Biomater Oral Craniomaxillofacial Appl 17:62–77

3. Wennerberg A, Albrektsson T (2009) Effects of titanium surface topography on bone integration: a systematic review. Clin Oral Implants Res 20:172–184

4. Ramazanoglu M, Oshida Y (2011) Osseointegration and bioscience of implant surfaces-current concepts at bone-implant interface, Implant Dent. Rapidly Evol Pract:307–658

5. De Bruyn H, Christiaens V, Doornewaard R, Jacobsson M, Cosyn J, Jacquet W, Vervaeke S (2017) Implant surface roughness and patient factors on long-term peri-implant bone loss. Periodontol 2000(73):218–227

6. Shemtov-Yona K, Rittel D (2015) On the mechanical integrity of retrieved dental implants. J Mech Behav Biomed Mater 49:290–299

7. Shemtov-Yona K, Rittel D (2015) An overview of the mechanical integrity of dental implants. Biomed Res Int 2015

8. Faia-Torres AB, Guimond-Lischer S, Rottmar M, Charnley M, Goren T, Maniura-Weber K, Spencer ND, Reis RL, Textor M, Neves NM (2014) Differential regulation of osteogenic differentiation of stem cells on surface roughness gradients. Biomaterials 35:9023–9032. https://doi.org/10.1016/j.biomaterials.2014.07.015

9. Rosa MB, Albrektsson T, Francischone CE, Schwartz Filho HO, Wennerberg A (2012) The influence of surface treatment on the implant roughness pattern. J Appl Oral Sci 20:550–555

10. Albrektsson T, Wennerberg A (2004) Oral implant surfaces: Part 1--review focusing on topographic and chemical properties of

different surfaces and in vivo responses to them. Int J Prosthodont 17(5):536–543

11. Donoso MG, Méndez-Vilas A, Bruque JM, González-Martin ML (2007) On the relationship between common amplitude surface roughness parameters and surface area: Implications for the study of cell–material interactions. Int Biodeterior Biodegradation 59:245–251

12. Liu X, Chu PK, Ding C (2004) Surface modification of titanium, titanium alloys, and related materials for biomedical applications. Mater Sci Eng R Rep. https://doi.org/10.1016/j.mser.2004.11.001

13. Ramulu M, Kunaporn S, Arola D, Hashish M, Hopkins J (2000) Waterjet machining and peening of metals. J Press Vessel Technol 122:90–95

14. Lieblich M, Barriuso S, Ibáñez J, Ruiz-de-Lara L, Díaz M, Ocaña JL, Alberdi A, González-Carrasco JL (2016) On the fatigue behavior of medical Ti6Al4V roughened by grit blasting and abrasiveless waterjet peening. J Mech Behav Biomed Mater 63. https://doi.org/10.1016/j.jmbbm.2016.07.011

15. Le Guéhennec L, Soueidan A, Layrolle P, Amouriq Y (2007) Surface treatments of titanium dental implants for rapid osseointegration. Dent Mater 23:844–854

16. Vardiman RG, Kant RA (1982) The improvement of fatigue life in Ti-6Al-4V by ion implantation. J Appl Phys 53:690–694

17. Aparicio C, Gil FJ, Fonseca C, Barbosa M, Planell JA (2003) Corrosion behaviour of commercially pure titanium shot blasted with different materials and sizes of shot particles for dental implant applications. Biomaterials 24:263–273

18. Leinenbach C, Eifler D (2006) Fatigue and cyclic deformation behaviour of surface-modified titanium alloys in simulated physiological media. Biomaterials 27:1200–1208

19. Barriuso S, Chao J, Jiménez JA, García S, González-Carrasco JL (2014) Fatigue behavior of Ti6Al4V and 316 LVM blasted with ceramic particles of interest for medical devices. J Mech Behav Biomed Mater 30:30–40

20. Shemtov-Yona K, Rittel D (2014) Identification of failure mechanisms in retrieved fractured dental implants. Eng Fail Anal 38:58–65

21. Straub W, Sprecher C, Peters JA, Windler M (2002) Method for producing a surface structure, in particular on a surgical implant. U.S. Patent 6:482,076 B1

22. Barriuso S, Lieblich M, Multigner M, Etxeberria I, Alberdi A, González-Carrasco JL (2011) Roughening of metallic biomaterials by abrasiveless waterjet peening: Characterization and viability. Wear 270:634–639

23. Rajesh N, Veeraraghavan S, Babu NR (2004) A novel approach for modelling of water jet peening. Int J Mach Tools Manuf. https://doi.org/10.1016/j.ijmachtools.2004.01.010

24. Arola DD, McCain ML (2000) Abrasive waterjet peening: A new method of surface preparation for metal orthopedic implants. J Biomed Mater Res. https://doi.org/10.1002/1097-4636(200009)53:5<536::AID-JBM13>3.0.CO;2-V

25. Arola D, McCain ML, Kunaporn S, Ramulu M (2001) Waterjet and abrasive waterjet surface treatment of titanium: A comparison of surface texture and residual stress. Wear 249:943–950. https://doi.org/10.1016/S0043-1648(01)00826-2

26. Arola D, Alade AE, Weber W (2006) Improving fatigue strength of metals using abrasive waterjet peening. Mach Sci Technol 10:197–218. https://doi.org/10.1080/10910340600710105

27. Sadasivam B, Hizal A, Arola D (2009) Abrasive waterjet peening with elastic prestress: A parametric evaluation. Int J Mach Tools Manuf 49:134–141

28. Sonntag R, Reinders J, Gibmeier J, Kretzer JP (2015) Fatigue performance of medical Ti6Al4V alloy after mechanical surface treatments. PLoS One 10:e0121963

29. Perec A, Radomska-Zalas A, Fajdek-Bieda A (2021) Experimental research into marble cutting by abrasive water jet. Facta Univ. Ser. Mech. Eng

30. Perec A, Radomska-Zalas A, Fajdek-Bieda A, Pude F (2022) Pocess optimization by applying the response surface methodology. In: (RSM) To the abrasive suspension water jet cutting of phenolic composites. Facta Univ. Ser. Mech. Eng

31. Fujisawa N, Takano S, Fujisawa K, Yamagata T (2018) Experiments on liquid droplet impingement erosion on a rough surface. Wear 398–399:158–164. https://doi.org/10.1016/j.wear.2017.12.003

32. Heymann FJ (1970) Erosion by liquids. Mach Des 10:118–124

33. Thomas GP, Brunton JH (1970) Drop Impingement Erosion of Metals. Proc. R. Soc. A Math. Phys. Eng Sci. https://doi.org/10.1098/rspa.1970.0022

34. Bowden JE, Field FP (1964) The brittle fracture of solids by liquid impact, by solid impact, and by shock. Proc R Soc London Ser A Math Phys Sci. https://doi.org/10.1098/rspa.1964.0236

35. Foldyna J (2011) Use of acoustic waves for pulsating water jet generation, in: acoust. Waves - From Microdevices Helioseismol. https://doi.org/10.5772/18862

36. Hloch S, Srivastava M, Nag A, Muller M, Hromasová M, Svobodová J, Kruml T, Chlupová A (2020) Effect of pressure of pulsating water jet moving along stair trajectory on erosion depth, surface morphology and microhardness. Wear:452–453. https://doi.org/10.1016/j.wear.2020.203278

37. Nag A, Hloch S, Čuha D, Dixit AR, Tozan H, Petrů J, Hromasová M, Müller M (2019) Acoustic chamber length performance analysis in ultrasonic pulsating water jet erosion of ductile material. J Manuf Process 47:347–356. https://doi.org/10.1016/j.jmapro.2019.10.008

38. Nag A, Hvizdos P, Dixit AR, Petrů J, Hloch S (2021) Influence of the frequency and flow rate of a pulsating water jet on the wear damage of tantalum. Wear 477:203893. https://doi.org/10.1016/j.wear.2021.203893

39. Srivastava M, Hloch S, Gubeljak N, Milkovic M, Chattopadhyaya S, Klich J (2019) Surface integrity and residual stress analysis of pulsed water jet peened stainless steel surfaces. Meas J Int Meas Confed 143. https://doi.org/10.1016/j.measurement.2019.04.082

40. Srivastava M, Hloch S, Krejci L, Chattopadhyaya S, Gubeljak N, Milkovic M (2022) Utilizing the water hammer effect to enhance the mechanical properties of AISI 304 welded joints. Int J Adv Manuf Technol 119:2317–2328. https://doi.org/10.1007/s00170-021-08357-9

41. Srivastava M, Nag A, Krejčí L, Petrů J, Chattopadhyaya S, Hloch S (2021) Effect of periodic water clusters on aisi 304 welded surfaces. Materials (Basel) 14:1–12. https://doi.org/10.3390/ma14010210

42. Stolárik G, Nag A, Petrů J, Svobodová J, Hloch S (2021) Ultrasonic Pulsating Water Jet Peening: Influence of Pressure and Pattern Strategy. Materials (Basel) 14:6019

43. Poloprudský J, Chlupová A, Šulák I, Kruml T, Hloch S (2021) Surface and Subsurface Analysis of Stainless Steel and Titanium Alloys Exposed to Ultrasonic Pulsating Water Jet. Materials (Basel) 14:5212

44. Hloch S, Souček K, Svobodová J, Hromasová M, Müller M (2022) Subsurface microtunneling in ductile material caused by multiple droplet impingement at subsonic speeds. Wear 490–491:204176. https://doi.org/10.1016/j.wear.2021.204176

45. Hloch S, Adamčík P, Nag A, Srivastava M, Čuha D, Müller M, Hromasová M, Klich J (2019) Hydrodynamic ductile erosion of aluminium by a pulsed water jet moving in an inclined trajectory. Wear 428–429:178–192. https://doi.org/10.1016/j.wear.2019.03.015

46. Srivastava M, Hloch S, Krejci L, Chattopadhyaya S, Dixit AR, Foldyna J (2018) Residual stress and surface properties of stainless steel welded joints induced by ultrasonic pulsed water jet peening. Measurement 127:453–462. https://doi.org/10.1016/j.measurement.2018.06.012

47. Poloprudský J, Nag A, Kruml T, Hloch S (2022) Effects of liquid droplet volume and impact frequency on the integrity of Al alloy AW2014 exposed to subsonic speeds of pulsating water jets. Wear 488–489. https://doi.org/10.1016/j.wear.2021.204136

48. Stolárik G, Svobodová J, Klichová D, Nag A, Hloch S (2023) Titanium surface roughening with ultrasonic pulsating water jet. J Manuf Process 90:341–356

49. Shah FA, Trobos M, Thomsen P, Palmquist A (2016) Commercially pure titanium (cp-Ti) versus titanium alloy (Ti6Al4V) materials as bone anchored implants—Is one truly better than the other? Mater Sci Eng C 62:960–966

50. Ottria L, Lauritano D, Andreasi Bassi M, Palmieri A, Candotto V, Tagliabue A, Tettamanti L (2018) Mechanical, chemical and biological aspects of titanium and titanium alloys in implant dentistry. J Biol Regul Homeost Agents 32:81–90

51. Huynh V, Ngo NK, Golden TD (2019) Surface activation and pretreatments for biocompatible metals and alloys used in biomedical applications. Int J Biomater 2019:3806504. https://doi.org/10.1155/2019/3806504

52. Nag A, Dixit AR, Petrů J, Váňová P, Konečná K, Hloch S (2022) Maximization of wear rates through effective configuration of standoff distance and hydraulic parameters in ultrasonic pulsating water jet, Facta Univ. Ser Mech Eng. https://doi.org/10.22190/FUME220523045N

53. Nag A, Stolárik G, Svehla B, Hloch S (2021) Effect of water flow rate on operating frequency and power during acoustic chamber tuning. In: Advances in manufacturing engineering and materials ii: proceedings of the international conference on manufacturing engineering and materials (ICMEM 2020). Springer International Publishing, Nový Smokovec, Slovakia, pp 142–154

54. Nag A, Hloch S, Dixit AR, Pude F (2020) Utilization of ultrasonically forced pulsating water jet decaying for bone cement removal. Int J Adv Manuf Technol. https://doi.org/10.1007/s00170-020-05892-9

55. Krystek M (1996) A fast Gauss filtering algorithm for roughness measurements. Precis Eng 19:198–200

56. Gadelmawla ES, Koura MM, Maksoud TMA, Elewa IM, Soliman HH (2002) Roughness parameters. J Mater Process Technol 123:133–145

57. Gorji NE, O'Connor R, Brabazon D (2021) XPS, SEM, AFM, and Nano-Indentation characterization for powder recycling within additive manufacturing process. IOP Conf Ser Mater Sci Eng 1182:012025. https://doi.org/10.1088/1757-899X/1182/1/012025

58. Schwarz F, Wieland M, Schwartz Z, Zhao G, Rupp F, Geis-Gerstorfer J, Schedle A, Broggini N, Bornstein MM, Buser D (2009) Potential of chemically modified hydrophilic surface characteristics to support tissue integration of titanium dental implants. J Biomed Mater Res Part B Appl Biomater An Off J Soc Biomater Japanese Soc Biomater Aust Soc Biomater Korean Soc Biomater 88:544–557

59. Tavakoli J, Khosroshahi ME (2018) Surface morphology characterization of laser-induced titanium implants: lesson to enhance osseointegration process, Biomed. Eng Lett 8:249–257

60. Chlupová A, Hloch S, Nag A, Šulák I, Kruml T (2023) Effect of pulsating water jet processing on erosion grooves and microstructure in the subsurface layer of 25CrMo4 (EA4T) steel. Wear 525:204774. https://doi.org/10.1016/j.wear.2023.204774

61. Lehocká D, Klichová D, Foldyna J, Hloch S, Hvizdoš P, Fides M, Botko F (2017) Comparison of the influence of acoustically enhanced pulsating water jet on selected surface integrity characteristics of CW004A copper and CW614N brass. Meas J Int Meas Confed 110. https://doi.org/10.1016/j.measurement.2017.07.005